Published in final edited form as:
ACS Appl Mater Interfaces. 2017 March 29; 9(12): 11095–11105. doi:10.1021/acsami.6b13624.

Suppressing Crack Formation in Particulate Systems by Utilizing Capillary Forces

Monica Schneider[†], **Johannes Maurath**[†], **Steffen B. Fischer**[†,‡], **Moritz Weiß**[†,‡], **Norbert Willenbacher**[†], and **Erin Koos**[*,†,‡]

[†]Institute for Mechanical Process Engineering and Mechanics, Karlsruhe Institute of Technology, Gotthard-Franz-Straße 3, 76131 Karlsruhe, Germany

[‡]Department of Chemical Engineering, KU Leuven, Celestijnenlaan 200f, 3001 Leuven, Belgium

Abstract

Cracks, formed during the drying of particulate films, can reduce the effectiveness or even render products useless. We present a novel, generic approach to suppress crack formation in thin films made from hard particle suspensions, which are otherwise highly susceptible to cracking, using the capillary force between particles present when a trace amount of an immiscible liquid is added to a suspension. This secondary liquid preserves the particle cohesion, modifying the structure and increasing the drying rate. Crack-free films can be produced at thicknesses much greater than the critical cracking thickness for a suspension without capillary interactions, and even persists after sintering. This capillary suspension strategy is applicable to a broad range of materials including suspensions of metals, semiconductive and ceramic oxides or glassy polymeric particles and can be easily implemented in many industrial processes since it is based on well-established unit operations. Promising fields of application include ceramic foils and printed electronic devices.

Keywords

crack formation; capillary suspensions; drying; wetting; solvent effects

Corresponding Author, erin.koos@kuleuven.be.

ORCID

Monica Schneider: 0000-0001-7422-0880
Johannes Maurath: 0000-0002-3491-2708
Steffen B. Fischer: 0000-0002-1595-4160
Moritz Weiß: 0000-0002-1647-3860
Erin Koos: 0000-0002-2468-2312

Author Contributions

M.S. designed and conducted the experiments with the TiO_2 and ZnO particles. J.M. designed the Al_2O_3 experiments and conducted them with M.W. S.B.F. aided with the conductivity measurements. N.W. and E.K. supervised this project and helped interpret the results. All authors were involved in analysis of data and completion of this paper. The authors declare no competing financial interest.

Notes

The authors declare no competing financial interest.

Europe PMC Funders Author Manuscripts

1 Introduction

Crack formation during drying is a ubiquitous phenomenon important in soil science as well as industrial material and processing development. Understanding crack formation in particle films and developing strategies to suppress crack formation is an important field of research, as desired product properties generally decline with the occurrence of cracks.1,2 Dried mud, paint coatings, ceramics and many other materials can show cracking during and after solvent evaporation. However, cracking is of utmost importance in hard particle coatings, such as those used in, for example, printed electronic devices such as battery electrodes,3 photonic crystals or antireflective coatings,4,5 filtration operations, as well as the processing of catalysts and ceramic materials,6 all of which are plagued by this phenomenon.

During the drying process, evaporation leads to solvent retention into the particle network. Menisci form between the particles at the liquid–gas–solid interface, inducing capillary forces and a capillary pressure. The capillary pressure p_c can be expressed by

$$p_c = \frac{2\gamma\cos\theta}{r_p} \quad (1)$$

assuming a cylindrical pore with radius r_p is wetted by a solvent with wetting angle θ and surface tension γ.7 Hence, a decreasing pore size results in a higher capillary pressure, which acts on the particles and pulls them together. In real systems, pore sizes vary and broad distributions lead to a more pronounced inhomogeneity in the resulting drying stress. 8–11 This capillary pressure also changes during drying as the distance between particles becomes smaller. As this capillary pressure overcomes other forces, such as the compressive stress, cracks form in the film.

There have been many strategies that have been put forth in recent years to reduce cracking. Variations in particle size, shear modulus, interparticle forces, and thermodynamic properties such as temperature, humidity, or gas flow rate, have all been shown to affect the shape and appearance of cracks.12 Rheological properties, such as the yield stress of the suspension, and vibrational preconditioning of the paste have also been shown to correlate with crack development.13 For biological and biomimetic materials, a spatial variation of the elastic moduli on the microscopic scale has shown to affect and hinder crack propagation.14

Because of to the generally high shear modulus of inorganic particles, corresponding suspensions are more prone to exhibit cracking during processing. These crack morphologies are dependent on the particle shape as well as any microstructure formed by a percolated network as these particles dry.15 Common solutions proposed to achieve fracture-free layers from suspensions include the use of soft particles with a sufficiently low glass transition temperature to allow for a relaxation of the drying induced interparticle tensile stress by deformation, the addition of a plasticizer, polymer, or a blend of soft and hard particles to provide the required deformability of the particles.16–18 The use of a soft substrate, or changing other substrate properties such as the wetting and roughness, can also

reduce crack formation.19 Another approach is to coat a colloidal precursor. The evaporation of the solvent leads to an in–situ growth of the particles, which replaces the arising void volume and thus avoids crack formation while drying.20,21 Sometimes, however, the specific material composition is restricted. In these cases, multistep coating procedures, increased drying time, or a method of inducing colloidal crystallization during coating can be used to reduce cracking.18,22,23 Using a multistep approach or long drying times can be time consuming and costly, however.

The particles can also be incorporated into an existing gel matrix or cracks can be reduced through attractive interactions causing the formation of a percolating particle network.24–26 In certain applications, however, residual components, for example, a polymeric binder, can be undesirable.27 Jin et al. also showed that the incorporation of emulsion drops can be used to decrease the amount of cracking.28 In this case, increased fractions of the dispersed fluid slowed the rate of air invasion, which may have accounted for the observed change in the cracking pattern. Since the emulsion fluid can be completely removed (though some residue from the surfactant will still be present), the method of Jin et al. is a versatile method to control cracking. A method that combines the use of a secondary fluid (without surfactants) and an induced particle network, should be an even more powerful approach, particularly when the final material composition is strictly limited.

Various relations have been proposed to describe the critical cracking thickness (CCT, h_{max}). 24,29–31 These relations focus on capillary pressure, particle shear modulus, and size, as well as particle coordination number and packing properties of the film. However, other important aspects like drying conditions, substrate properties or the effect of additives are not considered. Moreover, such models are restricted to specific boundary conditions, such as stress- or strain-limited drying regimes. Therefore, such relations are of limited use for quantitative predictions of CCT and it is often better to directly measure the maximum film height for each system at the specified conditions.

Here, we present a generic novel strategy to suppress crack formation during drying of particle suspensions by taking advantage of capillary forces inferred via the addition of a small amount of a second liquid that is immiscible with the main or bulk fluid of the suspensions. Such ternary particle–liquid–liquid systems are termed capillary suspensions. 32,33 Capillary forces can lead to the formation of a particulate gel comprising a sample-spanning particle network, regardless of whether the secondary liquid wets the particles better or worse than the bulk phase.32 Two types of capillary suspensions are distinguished depending on the two-liquid wetting angle $\theta_{2/}$ that the secondary liquid forms against the solid surface in the bulk phase environment. In the pendular state ($\theta_{2/} < 90°$), the secondary liquid wets the solid phase better than the continuous phase and forms pendular shaped bridges between the particles. In the case where $\theta_{2/} > 90°$, termed the capillary state, the particles form clusters around small volumes of the second liquid.34 Reported technical applications of capillary suspensions cover a broad range of materials and products including novel food products, such as heat stable or low calorie chocolate spreads,35,36 pastes for printed electronics like, for example, slot-die-coated lithium-ion battery electrodes37 or front contacts of solar cells with high shape accuracy,27 capillary

suspension-based foams38 as well as precursor for highly porous ceramic and glass membranes.39

In this Research Article, we focus on pendular state capillary suspensions and demonstrate how crack formation is suppressed and drying is accelerated in these systems. A pendular shaped liquid bridge exerts a capillary force F_c between two adjacent particles of same radius R is given by

$$F_c = 2\pi R \gamma_{2l} \cos\theta_{2l} \quad (2)$$

with the assumptions that the particle separation is zero and the liquid bridge, with the interfacial tension γ_{2l}, is smaller than the particle size.40,41 More generally, the force will depend on the volume of the liquid bridge as well as the filling angle and the shape of the droplet.42,43 Further corrections can be included for particles that are not in contact and for rough particles.44,45 Generally, the capillary attraction is significantly higher and acts over larger distances than the omnipresent van der Waals force.32 The influence of charge occurs at a very short range and can slow or even prevent particles from approaching. When a bridge does form, the affinity of the interface to the solid surface (e.g. from van der Waals and electrostatic forces) can modify the profile of the drop within a range up to 100 nm. 46,47 The macroscopic contact angle and macroscopic attraction is not affected by this core region, however. The influence of the charge in combination with a capillary interaction depends on the wettability of the surface. Yamamoto et al. showed that the interaction between micronsized polymer spheres and a silicon wafer with water adsorbed to the surfaces depends on the wafer surface treatment.48 Hydrophobic surfaces showed an electrostatic interaction at all distances, while the interaction for hydrophilic surfaces changed from electrostatic at long distances to capillary at short distances.

Suspended particles connected by pendular bridges can assemble into sample-spanning networks even at low particle volume fractions ϕ. Such particulate gels then exhibit a yield stress σ_y, which for equally sized particles is given by

$$\sigma_y = f(\phi)\, g(S, \tilde{s})\, \frac{\gamma_{2l} \cos\theta_{2l}}{R} \quad (3)$$

where the number of contacts per particle is captured by the function $f(\phi)$.49,50 The normalized particle separation $\tilde{s} = s/R$ is considered in the term $g(S, \tilde{s})$ along with the amount of secondary liquid added to the suspension, described by the saturation S32,51

$$S = \frac{V_{\text{wetting fluid}}}{V_{\text{total fluid}}} \quad (4)$$

The thermodynamics of drying capillary suspensions are very complex. Mass transfer is influenced by numerous parameters such as the diffusivity of the secondary liquid in the bulk fluid, the low solubility of the secondary liquid in the bulk phase, the Laplace pressure

in the liquid bridges or the equilibrium partial pressure of both liquid components in the ambient gas phase.52 The drying process of binary liquid mixtures in porous media has been investigated before, but research is essentially limited to miscible liquid combinations.53,54 This complexity can be used to tune the drying process allowing the morphology and drying rate to be controlled.

2 Experimental Section

2.1 Sample Production

To create the capillary suspensions, TiO_2 particles (Evonik, Aeroxid P25, Essen, Germany, average aggregate radius $R_{50,3}$ = 0.39 μm, polydispersity $(R_{90,3} - R_{10,3})/R_{50,3}$ = 2.62), ZnO particles (Evonik, VP ADnano ZnO, Essen, Germany, mean aggregate size according to supplier <0.18 μm), and hydrophobically modified $CaCO_3$ (Solvay, Socal U1S1, Salin de Giraud, France, $R_{50,3}$ = 0.9 μm, polydispersity of 1.54) were dispersed in n-octanol (Merck, Emplura, Darmstadt, Germany) and various volumes of distilled water were added as secondary liquid. For the infrared spectroscopy measurements, the distilled water was replaced by deuterium oxide D_2O (Carl Roth, Karlsruhe Deutschland). During sample preparation, the particles were slowly added to the bulk fluid while stirring at low speed with a turbulent beater blade (200 rpm), the mixture was then stirred at high speed (30 min, 1000 rpm) to ensure a homogeneous distribution. Finally, the capillary network formation was induced by adding varying amounts of the secondary liquid and maintaining the high stirrer speed for another 5 min. The solid volume fraction ϕ of the capillary suspensions were ϕ_{TiO_2} = 0.04, ϕ_{ZnO} = 0.05, and ϕ_{CaCO_3} = 0.10. The TiO_2 samples containing surfactant were prepared with 10 vol% aqueous surfactant solution (Evonik, Tego Dispers 752W, Essen, Germany) as secondary liquid.

The suspensions were coated on hydrophilic polyester foils with a doctor blade made of brass. The doctor blade gap height was 100 μm and accurate shapes were achieved by confining the pattern with a 60 μm thick adhesive tape to a square with 1 cm sides and making multiple passes. The blade was drawn over the polyester foil (Folex Coating GmbH, X-500, Cologne, Germany) with a constant velocity of 50 mm/s. This caused a shear rate of 300 s^{-1}, a value typical for screen printing. Additionally, this speed was chosen so that a smooth, homogeneous and continuous wet film was generated. The viscosity of the suspensions at the coating speed varied between 135 ± 4 mPa s for the sample without added water to a maximum of 550 ± 20 mPa s for the S = 0.05 samples (the viscosity for the higher saturation samples is lower than for the 5 % sample). Furthermore, multiple passes ensured that the wet films all had the same 160 μm thickness. The films were then left in the fume hood to dry at room temperature. Films with varying saturations were prepared and dried simultaneously. Humidity during drying varied slightly around 75 %. After a drying time of 48 h, the sample surfaces were analyzed in a scanning electron microscope (Hitachi, S-4500, Krefeld, Germany). The height profiles were examined with a 3D laser microscope (Keyence, VK-X100 Laser Microscope).

The ceramic discs were prepared with α-Al_2O_3 (Almatis, CT3000SG, Ludwighafen, Germany, $R_{50,3}$ = 0.34 μm, polydispersity of 2.40), paraffin oil as the bulk phase (Carl Roth, Karlsruhe, Germany) and a water-sucrose solution as secondary phase (Carl Roth, D(+)-

Sucrose, Karlsruhe, Germany, 1.835 M). Additionally, the suspension contained 0.5 vol% of the surfactant polysorbat 20 (Carl Roth, Tween 20, Karlsruhe, Germany) to avoid agglomeration. The solid volume fraction of the suspension was $\phi_{Al_2O_3} = 0.15$. The suspensions were stirred for 10 min at 1200 rpm with a turbulent beater blade, another 5 min after adding the surfactant, and again for 10 min at 800 rpm after adding the secondary phase. The final homogenization step was a 24-h ball mill treatment. The suspensions were coated on a porous Al_2O_3 substrate, followed by a thermal debinding procedure (30 min at 200 °C, 1 h at 500 °C and 15 min at 800 °C) and then sintered (2 h at 1550 °C). The magnified images were made with the 3D laser microscope.

Nickel films were used for conductivity measurements. The nickel powder (abcr GmbH, 100–150 nm Nickel Nano Powder, AB 254802, Karlsruhe Germany) was dispersed in 1-octanol with using a turbulent beater blade at 1000 rpm for 15 min. The suspensions were stirred again at 1000 rpm for 5 min after adding distilled water. The films were coated onto a glass substrate using a Universal Applicator (Zehntner, ZUA2000, Sissach, Switzerland) and dried overnight at 220 °C.

2.2 Characterization

The static three phase contact angle θ_{2l} was measured to characterize the solid–liquid–liquid systems. The particles were pressed to a dense tablet under a pressure of 19 MPa and sintered at 1000 °C for 5 h to achieve a densely packed structure. The sintered tablet was polished, placed in a glass container and covered with n-octanol. A droplet of distilled H_2O or D_2O was placed on the surface of the tablet using a syringe and the resulting three phase contact angle θ_{2l} evaluated via an image analysis program (Krüss, Drop Shape Analysis, Hamburg, Germany). The root mean squared surface roughness of the TiO_2 tablet was 0.33 $\pm$ 0.05 µm with an average distance between peak and valley of 0.8 $\pm$ 0.1 µm. Since the drops we used to measure the contact angles were much larger (mm), we ignored the effect of surface roughness. It should be stated that the difference in roughness of the particles compared to this substrate would change the effective contact angle. Additionally, the oxide surface may change with time or after it was heated during the sintering procedure. It is not our intention that this contact angle be used to directly calculate the interaction force, but rather this measured contact angle be used as an indication that the prepared suspensions were in the pendular state.

Infrared spectroscopy (Bruker, Tensor FT-IR 27) was performed using a diamond attenuated total reflection (ATR) crystal to determine the chemical composition of the capillary suspension film during drying. The suspensions were coated onto the ATR crystal with a defined shape of 5 $\times$ 5 mm^2 using a 100 µm doctor blade and an adhesive tape mask with the desired cut-out area. The infrared absorbance spectra of the pure substances were also measured as can be seen in Figure 1.

The yield stress of each suspension was determined with a rotational rheometer (Thermo Scientific, Mars II, Karlsruhe, Germany) and sandblasted plate/plate (35 mm diameter) geometry. By applying successively increasing stress values and measuring the resulting equilibrium deformation, two distinct linear regimes can be found in a double-logarithmic plot. The yield stress is then defined as the intersection of the two linear curve fits

representing the onset of irreversible deformation. The measurement error was estimated to be 10 % and includes the reproducibility of sample preparation and measurement.

Finally, the influence of cracking on the functionality of different films was characterized using permeability, filtration, and resistivity measurements. Permeability of ceramic membranes was measured using a pressure strainer (DrM, Maennedorf, Switzerland) where the volumetric flow rate was measured using an electronic balance. The experiment was conducted at room temperature using water with a pressure difference of 1.5 bar. The filtration tests used monomodal polystyrene particles with diameters of 1 and 5 μm (Micromer 01-00-103 and 01-00-503, Micromod Partikeltechnologie GmbH). The filtration was carried out at room temperature using 40 mL samples with a concentration of 1×10^{-4} g/mL. The filtration gauge pressure was 1.5 bar. Particle size distribution before and after filtration was obtained using dynamic light scattering (Zetasizer Nano ZS, Malvern). Bubble point tests were conducted following ISO 4793. The conductivity of nickel films was measured using a four-point probe with 3.96 mm diameter electrodes spaced inline at 10 mm. The voltage was supplied with a Voltcraft VLP-1303 Pro power supply and the current measured using a Benning MM9 multimeter. Conductivity was measured after films were coated onto a glass substrate and dried overnight at 220 °C.

3 Results and Discussion

Capillary suspensions promise a new formulation route for manufacturing crack-free particulate films because the capillary network can suppress stress induced, crack-forming particle migration during the drying process. Titanium oxide TiO_2 capillary suspensions with n-octanol as bulk phase and water as secondary liquid form a pendular state network with a three-phase contact angle of 79°. Thus, the secondary liquid forms pendular bridges between the particles creating a sample-spanning network that avoids sedimentation and further particle aggregation after dispersing. The SEM images in Figure 2a show the dry film surfaces of the pure TiO_2 suspension and the capillary suspensions with varying saturation S. The images clearly demonstrate that crack formation during drying is significantly suppressed upon addition of the secondary liquid. A difference in crack formation due to variations in the dry film thickness can be excluded here, as this quantity only varied between 15.6 and 17.4 μm for the sheets shown.

A simple quantification of the crack development can be achieved by binarization of the SEM images. The Minkowski number M_0 describes the area density of the cracks (the crack area divided by the total image area)55 and the resulting values are shown in Figure 2b as a function of saturation, quantitatively characterizing the reduced cracking. For the sample without added secondary liquid ($S = 0.00$), the SEM image reveals a high number of long cracks in the dried film. These cracks connect multiple domains and have a tip-to-tip length spanning the image. The surface morphologies of the dry particulate films change when adding increasing amounts of water to the TiO_2 suspension. The visible number of cracks is reduced and the size also changes to narrower and shorter cracks that no longer interconnect to form closed domains. These average crack widths are also shown in Figure 2b, where the error bars show the standard deviation for the crack widths. The average width decreases roughly linearly with saturation and the standard range of widths also decreases. The

successful formation of the capillary network is evident from the increasing yield stress as a function of the saturation S (Figure 2c). Without any added secondary liquid, the suspension yield stress is around 10 Pa and increases by an order of magnitude when adding up to 5 % of H_2O. With 7 % of secondary liquid in the capillary suspension, the cracks are hardly recognizable and M_0 reaches a minimum—decreasing by 2 orders of magnitude. However, spherical agglomeration occurs at saturations above the point of maximum network strength (as measured by the yield stress) indicated by the large, round aggregates, which are clearly visible for $S = 0.07$. This phenomenon has also been observed for other capillary suspension systems.56,57 Here, a small amount of surfactant added to the secondary liquid helps to avoid these aggregates, as shown in the bottom right image in Figure 2a without a significant decrease in the yield stress (star in Figure 2c).

The decrease in cracking is not due to variations in the film height, which was kept constant. Any changes due to differences in packing can also be excluded as the sheets had the same 160 μm height before drying and nearly uniform heights, 15.6–17.4 μm, with no trend in saturation, after drying. For the suspension without added secondary fluid, a CCT as low as 3 μm was measured. The films shown in Figure 2 are well above this critical value and the clear cracking observed in this film is consistent with this measurement. The CCT measured in the suspension without added liquid is lower than measured for other ceramic films,30,58 but those films had an aqueous bulk fluid, were dried under different conditions and contained polymeric binders. Since our film did not contain such additives, a lower CCT would be expected. Furthermore, the TiO_2 particles used here were agglomerates of smaller primary particles. This CCT can also be calculated for the pure suspension using various theories, but we would have to make assumptions about key parameters.24,30 These theoretical calculations also cannot be used to predict the CCT for the pendular state material systems since they do not include the contribution of capillary forces to the crack formation phenomenon. This contribution is clearly significant considering the dramatic increase in the critical cracking thickness for the capillary suspension over the suspension without added liquid.

The schematic in Figure 3 compares a stabilizer-free suspension with a capillary suspension in the wet film at various times during drying and serves as a hypothesis for the significant difference in the critical cracking thickness in capillary suspensions. Initially, both suspensions are completely covered by the bulk solvent. As the film begins to dry at $t_1 > 0$, the solvent recedes into the pores. Most of the solvent has evaporated at a much later time $t_2 \gg t_1$. The nonstabilized particles agglomerate resulting in a broad pore size distribution between particles and the agglomerates. In the case of the capillary suspension, the secondary liquid maintains the homogeneous particle distribution during the initial drying process causing more uniform pore diameters. At a constant bulk solvent contact angle θ and surface tension γ, the capillary pressure p_c in the pores is inversely proportional to the pore radius r_p where smaller pores lead to a higher capillary compression of the surrounding solid while drying.

Consequently, these variations in capillary pressure, which are caused by the broad pore size distribution across the sample volume, lead to huge anisotropic stress differences during the drying process that inevitably cause cracks.7,12 For the capillary suspensions investigated

here, the pendular bridges between the particles resist particle motion into compact domains and therefore provide a balanced drying stress across the sample surface. Therefore, the capillary pressure across the particulate film is uniform causing the number and size of cracks to diminish. The typical time for motion of the particles from the capillary bridges ($t_{capillary} \approx 96$ ns) is much shorter than the typical time for the bridge to evaporate ($t_{drying} \approx 500$ μs),9 so response of the network to changes in the drying front can be considered to be nearly instantaneous.

This change in the pore morphology, as well as the existence of a sample-spanning particle network, was shown in a previous microscopy study that used an index-matched model system.59 In that work, the direct bridging of the particles by the secondary fluid in the pendular state as well as clustering of particles in the capillary state are visible. Neighboring particles tend to be in contact (as evidenced by the location of the primary peak in the pair distribution function) with adjacent particles separated by a distance slightly less than four particle radii. This particle separation is fairly uniform for each of the capillary suspensions imaged in that work. Furthermore, the existence of a multiply connected sample-spanning particle network where two particles are connected through at least one pathway was shown in the 3D images.59 This particle network would significantly reduce particle migration since any motion by a single particle would require movement of multiple other particles. Since the capillary bridges are much stronger than other types of interparticle forces,32,34 this movement is greatly hindered.

In the stress-limited regime, the critical crack thickness is given by a balance between the elastic energy and the increased surface energy.30 Usually, this maximum stress is given by the maximum capillary pressure ($-P_{max} \propto R^{-1}$),60 but in this case, the capillary pressure is opposed by the bridging capillary interactions with a yield stress $\sigma_y \propto R^{-1}$.50,61 This means that the capillary pressure and the yield stress both have the same dependence on the particle size. Therefore, we do not expect the capillary interactions to change the relationship between the CCT and particle size.30,31 Air invasion also occurs via bursting rather than cracking for large particles.62 The capillary network also resists such particle motion, so this bursting may be reduced as well. The capillary suspensions may also be affected by surface charge. Such a charge is expected to weaken the capillary interaction in the wet state48 and decrease the final packing fraction when the film is dry.60 The influence of particle surface charges, however, seems to be small for the systems investigated here. A strong increase in yield stress occurs when the secondary fluid is added, that is, capillary bridges form and their force is quite strong despite of potentially counteracting surface charge effects. Electrostatic interactions will not have an effect on the suspension without added water.

To gain more insight into the change of sample composition while drying, infrared spectroscopy has been employed revealing a distinct change in drying velocity because of the presence of the secondary fluid in the samples. The films were coated onto an attenuated total reflection (ATR) crystal and the resulting absorption intensity of the infrared light as a function of the wavenumber ν and time is depicted in Figure 4a–c. The absorbance spectra of the pure substances can be found in Figure 1. The suspensions were prepared with deuterium oxide D_2O as secondary liquid with a clearly distinguishable peak at 2476 cm^{-1} not interfering with the n-octanol absorption peaks, for example, the methylene stretching

resonance frequency ν_{CH_2} = 2930 cm^{-1} and the alcohol specific OH-band at ν_{OH} = 3330 cm^{-1}.63 TiO_2 shows resonance at a frequency of ν_{TiO_2} = 419 cm^{-1} presumably corresponding to the Ti-O lattice vibration. 64,65 The area under each characteristic resonance peak was calculated for $\nu_i \pm 20$ cm^{-1} and plotted as a function of time in Figure 4d-f. Significant differences can be found for the drying kinetics depending on saturation. The time-resolved absorption spectra for the sample with $S = 0$ are shown in Figure 4a and d. After 81 min, the absorption at the characteristic frequencies ν_{OH} (3330 cm^{-1}) and ν_{CH_2} (2930 cm^{-1}), indicating the residual solvent, has disappeared. The dry film state is reached and the only remaining peak visible, at a wavelength of 419 cm^{-1}, is attributed to the solid TiO_2. The maximum of the TiO_2 peak intensity at approximately 60 min is due to a superposition of contributions from all components in this frequency range and does not correspond to any changes in the Ti-O lattice. The time at which only the TiO_2 peak remains and the intensity of this peak is constant is assumed to correspond to the state where the thin film is completely dry. Adding D_2O to the suspension shows a decrease of the drying time, with $S = 0.03$, the dry state is reached after 75 minutes (Figure 4b and e), and this is further reduced to 42 min for $S = 0.05$ (Figure 4c and f).

To understand how the addition of a secondary fluid reduces the time to evaporate the bulk solvent, we assume that the bulk fluid evaporates first. The negative Laplace pressure due to the concave shape of the pendular bridges and the interfacial tension (8.52 mN/m) 66 between the two liquids prevents the rapid evaporation of the secondary liquid, keeping the water trapped in the pendular bridges until the bulk octanol surrounding the bridges is removed. These bridges remain during the initial drying steps holding the particles in their initial position corresponding to a homogeneous interparticle pore size distribution during the drying process. This hypothesis is complicated by the lower vapor pressure at ambient conditions of the n-octanol ($p_{v,\ octanol,\ 20°\ C}$ = 0.031 mbar, $p_{v,\ H_2O,\ 20°\ C}$ = 23.37 mbar) and the low, but measurable solubility of water in octanol (48.67 ± 0.50 mg/g at 20 °C).67 While this solubility corresponds to a saturation of $S = 0.039$, the actual amount of water dissolved in the octanol would be much lower given the slow dissolution rate and thermodynamic stability of concave bridges. As the bridges between particles are filled with the solvent (water) with a higher vapor pressure, the total drying time decreases with increasing amount of secondary fluid. This effect, however, is not as great as the large reduction in drying time seen in the IR absorbance spectra in Figure 4. It should be noted, however that the dissolution will be affected by the bridge size both when these bridges are surrounded by the secondary liquid and when surrounded by air. The smaller droplets are thermodynamically more stable than the larger droplets, but difference in force for these drops is more sensitive to small changes in volume.

Generally, the initial mass transfer during drying is not influenced by the particle packing unless the solid volume concentration exceeds 60-75 %, below which the evaporation rate of the suspension is comparable to the evaporation rate of the pure bulk fluid.68,69 This contradicts the obviously enhanced drying rate for capillary suspensions (Figure 4). Drying of particulate systems underlies a capillary diffusion limited regime, when the solvent recedes into the pores. Thus, an increased solvent mass transfer for the capillary suspensions might be attributed to the improved wetting of the capillaries due to hydrogen bonds that can be formed between n-octanol and water.70,71 Alternatively, the evaporation rate can also be

reduced by skin formation on the film surface.72,73 In the pure suspension, a fraction of fine TiO_2 particles (primary particle size ~25 nm) might be able to diffuse within the solvent due to low interparticle forces and decrease evaporation rate when forming a packed layer at the evaporation front as in the formation of coffee rings.74,75 In the capillary suspension, the particles are trapped by the secondary liquid and are unable to follow the evaporation front. This striking change in evaporation rate will be addressed in future research.

The formation of capillary suspensions is a generic phenomenon and has been observed for a large number of particle–liquid–liquid combinations.32,33 The change in drying and crack formation has also been investigated using other materials besides the TiO_2 system discussed above. For example, the surface of dry films made from zinc oxide capillary suspensions (ZnO in octanol, $\phi = 0.05$, with added water) exhibits a similar reduction in crack formation with increasing saturation (Figure 5a). In this system, the cracking is almost completely prevented at $S = 0.05$ with very little spherical agglomeration. The example with ZnO was in the pendular state, but this reduction in cracking caused by the capillary force can also be observed in the capillary state, where the secondary liquid does not preferentially wet the particles. In the example shown in Figure 5b, hydrophobically modified $CaCO_3$ is dispersed in octanol ($\phi = 0.10$) with added water. Since the preferentially wetting liquid is the majority liquid, the sample without added liquid has $S = 1.00$, and $S = 0.97$ with 3 vol% added water. This capillary state system shows large cracks without added water, but no cracks when water is added. Once again, the cracking was not due to differences in the film height since both films have a dry film thickness of 20 μm. The network formed in the capillary state can be a mixture of strong capillary and relatively weak van der Waals interactions.59 Therefore, we still expect mixing conditions to be more critical in the capillary state.76 The reduction in cracking in the capillary state may also be more sensitive to the drying conditions as the energy balance forcing the particle–liquid–liquid system to form a stable capillary suspension may not be valid anymore when the surrounding bulk fluid is totally evaporated due to the sensitivity of this state to the contact angle. 34 This can significantly weaken the attractive force during the later drying stages. Despite these shortcomings, a reduction in cracks in both pendular and capillary state systems can be demonstrated.

The particle volume fraction is also expected to influence the observed cracking. In the case where no secondary liquid is present, either a thinner region is observed in the center of the sample (e.g., in the TiO_2 suspension) as the particles flow toward the edge of the drop where they form a compact region, or the film shrinks and a denser layer is observed (e.g. in the Al_2O_3 suspension). The former case should result in the observed cracks becoming thicker and with a wider spacing at higher volume fractions.26 In the latter case, the amount of shrinkage should change with the volume fraction, meaning that the final film may be above or below h_{max} depending on the geometric restrictions. In capillary suspensions, the shrinkage of the film is reduced (or nonexistent) and no particle mobility toward the edges is observed. This observation is consistent with the case that the initial (pinning) and intermediate (packing) drying being replaced by the final (percolation) stage in the capillary suspension samples where a percolating particle network is already present. Therefore, the presence of the capillary network is expected to have a more pronounced effect at low volume fractions. However, crack formation can be significantly reduced even in suspensions with particle loading as high as $\phi = 0.15$ as shown for the Al_2O_3 system below.

The reduction in crack formation was investigated in the previous examples using an n-octanol/H_2O system. This reduction can also be observed using paraffin oil as bulk phase and a water-sucrose solution as secondary phase for Al_2O_3 (Figure 6). In this case, the solid volume fraction ($\phi = 0.15$) was higher than the previous examples and even thicker (300 μm wet film) crack-free layers were obtained. These layers are coated onto a porous ceramic substrate, debinded to remove the liquids and then sintered. The bulk fluid is removed through suction into the porous substrate in addition to evaporation during debinding. This suction can be treated as an “accelerated drying”, where capillary forces still play an important role as in conventional air drying processes (e.g., the evaporation of octanol in water in the systems discussed above). The film thickness after debinding was 193 μm for the pure suspension and 290 μm for the capillary suspension. The film from the pure suspension becomes even thinner and denser during sintering (175 μm, porosity $\epsilon \approx 35\%$) than for the capillary suspension (290 μm, $\epsilon = 55 \pm 2\%$). This density results from settling of particles in the weak particle network of pure suspensions during debinding and sintering. Dittmann et al. already observed a lower porosity and consequently a stronger shrinkage of ceramics based on pure suspensions compared to ceramics made from capillary suspensions.39 Such a change in the final porosity of the debinded film could change the CCT,31 but this effect is minor compared to the influence of the capillary network itself. The crack-free capillary suspension film shown in Figure 6 is more than 6 times greater than the CCT for the suspension without added liquid (46 μm in the debinded state). While a change in porosity should affect h_{max}, our measured values for the CCT clearly show that the bridges increase this value by much more than would be predicted for the change in porosity alone. Therefore, the bridges are clearly beneficial for reducing cracks.

The use of a capillary suspension prevented the formation of cracks on the surface after debinding and this crack-free surface even persisted after sintering. SEM images of the film cross section for ceramic films made from pure suspensions show that the cracks extend through the film thickness and there is even partial delamination of the film from the substrate near the crack. The particle migration was restricted in the capillary suspension following drying and during the initial stages of debinding by the presence of sucrose in the secondary fluid, which crystallized at the particle contacts. The persistence of this crack-free nature in capillary suspensions, even during sintering when all of the secondary fluid has been removed, is likely due to the sample-spanning particle network where particles are connected to multiple neighbors.59

In the example shown in Figure 6, the 300 μm films were coated onto a sintered Al_2O_3 substrate with height of 2 mm and porosity of $53 \pm 2\%$. Such layered, or asymmetric, membranes are used in particle filtration and gas separation where a thin filtration layer is used to maximize the flow rate while ensuring sufficient mechanical strength.77 The difference in cracking has a significant impact on the performance of the filter. Permeability measurements show that the sample with cracks made without secondary liquid ($S = 0.000$) has the same permeability as the substrate (39.1 ± 6.4 $m^3/(m^2 \cdot h \cdot bar)$ versus 38.2 ± 1.3 $m^3/(m^2 \cdot h \cdot bar)$ for the substrate). The sample with added liquid ($S = 0.015$) has a much lower permeability of 12.1 ± 3.9 $m^3/(m^2 \cdot h \cdot bar)$. The same trend in permeability was also confirmed for thinner (100 μm) layers. The film created from the pure suspension had clear cracks and a permeability of 38.9 ± 1.5 $m^3/(m^2 \cdot h \cdot bar)$, whereas the capillary suspension

layer had no visible cracks and a permeability of 26.2 ± 1.3 $m^3/(m^2 \cdot h \cdot bar)$. In the capillary suspension samples, the much lower permeability shows that top layer is intact and can still be used for particle separation. The layers created without secondary fluid are nonfunctional as small particles would readily pass through the large cracks to the substrate.

This loss in functionality is clearly evident in the filtration tests shown in Figure 7. Monomodal polystyrene particles with a diameter of 1 μm can be successfully separated by the 100 μm (wet film) capillary suspension based membrane, whereas the membrane made from the pure suspension was not able to separate 5 μm particles because of the large macroscopic cracks. The pore diameter for the pure suspension sample is $d_{50,3}$ = 1.2±0.1 μm and $d_{10,3}$ = 0.46 ± 0.03 μm. The membrane made from the capillary suspensions exhibits an average pore size of $d_{50,3}$ = 4.0 ± 0.2 μm and $d_{10,3}$ = 1.7 ± 0.01 μm. The pore sizes were measured through image analysis of crosscut SEM images, which can overestimate the pore size compared to other common methods (e.g., Hg-porosimetry).39,56 Consequently direct correlations between cutoff determined by filtration tests and pore size from image analysis are not possible. Nevertheless, it should be easier to separate 1 μm particles with the sample without added secondary phase than with the capillary suspension sample, since the $d_{10,3}$, which should roughly correspond the size of the neck between pores—the limiting length scale for particles to pass through the filter—is significantly smaller. The failure of this membrane is obviously due to the large cracks present. This is further confirmed using a bubble-point test, which measured a pore size of 6.7 ± 0.1 μm for the film sample. This pore size is close to that of the substrate itself (7.4 ± 0.3 μm), indicating that the cracks cause this film to have a negligible impact on particle filtration.

A similar loss of function with cracking can also be seen for conductive films like the Ni layers investigated here. Increased cracking can decrease the conductivity of a film by lengthening the effective distance between two points due to the creation of tortuous percolation pathways while reducing the number and effective cross-sectional area of these pathways.78 The conductivity will decrease to zero when the domains become detached. Six nickel films prepared from pure as well as capillary suspensions were dried but not sintered to test the impact of cracking on the conductivity as shown in Figure 8. Thinner films, both without cracks, with a thickness near 130 μm had similar conductivities ($\sigma_{S=0.00}$ = 8.9 ± 0.1 × 10^{-5} S·m^{-1} and $\sigma_{S=0.05}$ = 1.1 ± 0.1 × 10^{-4} S·m^{-1}). As the film thickness increases, the conductivity should also increase due to the increasing effective conductive area. This increase is clearly shown in the films made from capillary suspensions where the conductivity increases linearly with the film thickness. The increase is also demonstrated for the intermediate thickness film made from the pure suspension ($h_{S=0.00}$ = 166 ± 9 μm, $\sigma_{S=0.00}$ = 1.2 ± 0.1 × 10^{-4} S·m^{-1}). However, the conductivity remains unchanged for the thicker film ($h_{S=0.00}$ = 227 ± 14 μm, $\sigma_{S=0.00}$ = 1.4 ± 0.1 × 10^{-4} S·m^{-1}). This is due to the development of cracks in the film without added liquid at a critical cracking thickness (CCT) between 160 and 200 μm. These cracks did not extend through the entire thickness of the film, but still increase the effective conductive pathway. As such, this thicker film did not show the same increase in the conductivity as the crack free films made from capillary suspensions.

4 Conclusions

We have demonstrated a route to create crack-free particulate films with minimal processing and material cost just by adding small amounts of a secondary liquid to a suspension thus introducing capillary bridges between particles. Microscopy images reveal a remarkable change in the crack pattern of dry films made from suspensions with varying amounts of secondary liquid for TiO_2, ZnO, $CaCO_3$ and Al_2O_3 systems with crack-free films produced at thicknesses at least five times greater than the critical cracking thickness measured for the suspension without added liquid. The reduction in cracking is caused by the bridges between particles causing a more homogeneous distribution of pore sizes, which prevents the strong anisotropic stress differences that cause cracking. Furthermore, the bridges between particles further reduce particle mobility and increase the drying rate of the bulk solvent next to the substrate. The observed reduction in cracking even persists after sintering as shown for the Al_2O_3 thick films. This ceramic sample is significant since the solvents and drying conditions are very different than the other samples. This implies that there is some resilience for the reduction in cracking depending on the drying conditions, but a more complete study should be undertaken.

This reduction in cracking improves the functionality of the films as demonstrated using membranes for filtration as well as conductive films. The filtration membranes with cracks demonstrated the same permeability as the porous substrate implying that liquid (and particles) can easily flow through the large cracks, which traversed the entire film thickness. This was further demonstrated with a filtration test. The membrane created from the capillary suspension, which did not exhibit cracking, was able to separate 1 μm particles easily, whereas the membrane made from the pure suspension could not even separate larger 5 μm particles. The formation of cracks also interferes with the conductivity of printed films. Cracks increase the percolation path length or can even prevent a direction connection between locations. This decrease in conductivity was shown for nickel films made form pure suspensions that in contrast to films made from capillary suspensions showed cracking at film thicknesses exceeding 180 μm. The experiments conducted with the TiO_2 capillary suspensions clearly showed that the maximum crack-free sheet thickness for capillary suspensions far exceeds the CCT measured without any capillary interactions.

While this research concentrated on systems without any chemical reactions, this research can also be applied to systems where reactions between the two fluids or between one of the fluids and particles take place. Experiments in systems where the secondary fluid is polymerized or cross-linked have also been conducted.79,80 While the properties affecting the strength of the capillary interactions, that is, interfacial tension and contact angle, are modified during this process, a sample-spanning network of particles connected by the bridges is still present. In fact, this method can be combined with different chemical reactions, for example, a reducing agent, which can be used to reduce the oxidation of conductive particles. The explicit effect of particle charge should also be investigated. Given the counteracting factors of charge on the capillary interaction and on the final particle packing, a thorough study of the charge on the strength of the capillary networks and on crack formation should be undertaken.

Acknowledgement

We want to thank Dr. Sunyhung Kim for the fruitful discussions regarding the drying of suspensions and the stress development during drying. Special thanks also to Stefan Heissler for the support with the IR measurements.

Funding

Financial support was provided from the German Research Foundation (Deutsche Forschungsgemeinschaft) grant agreement no. KO4805/2-1 and the European Research Council under the European Union's Seventh Framework Program (FP/2007–2013)/ERC Grant Agreement no. 335380.

References

(1). Mathews N, Lam YM, Mhaisalkar SG, Grimsdale AC. Printing Materials for Electronic Devices. Int J Mater Res. 2010; 101:236–250.

(2). Juillerat F, Bowen P, Hofmann H. Formation and Drying of Colloidal Crystals Using Nanosized Silica Particles. Langmuir. 2006; 22:2249–2257. [PubMed: 16489814]

(3). Park J-H, Cho J-H, Park W, Ryoo D, Yoon S-J, Kim JH, Jeong YU, Lee S-Y. Close-Packed SiO_2/poly(methyl Methacrylate) Binary Nanoparticles-Coated Polyethylene Separators for Lithium-Ion Batteries. J Power Sources. 2010; 195:8306–8310.

(4). Bardosova M, Dillon FC, Pemble ME, Povey IM, Tredgold RH. Langmuir-Blodgett Assembly of Colloidal Photonic Crystals Using Silica Particles Prepared Without the Use of Surfactant Molecules. J Colloid Interface Sci. 2009; 333:816–819. [PubMed: 19251265]

(5). Prevo BG, Hon EW, Velev OD. Assembly and Characterization of Colloid-Based Antireflective Coatings on Multicrystalline Silicon Solar Cells. J Mater Chem. 2007; 17:791–799.

(6). Özgür C, Şan O. Fabrication of Superhydrophilic Membrane Filters Using Spherical Glass Particles Obtained by Ultrasonic Spray Pyrolysis. Ceram Int. 2011; 37:965–970.

(7). Zarzycki J, Prassas M, Phalippou J. Synthesis of Glasses from Gels: The Problem of Monolithic Gels. J Mater Sci. 1982; 17:3371–3379.

(8). Dufresne ER, Stark DJ, Greenblatt NA, Cheng JX, Hutchinson JW, Mahadevan L, Weitz DA. Dynamics of Fracture in Drying Suspensions. Langmuir. 2006; 22:7144–7147. [PubMed: 16893207]

(9). Dufresne ER, Corwin EI, Greenblatt NA, Ashmore J, Wang DY, Dinsmore AD, Cheng JX, Xie XS, Hutchinson JW, Weitz DA. Flow and Fracture in Drying Nanoparticle Suspensions. Phys Rev Lett. 2003; 91:224501. [PubMed: 14683242]

(10). Xu Y, German GK, Mertz AF, Dufresne ER. Imaging Stress and Strain in the Fracture of Drying Colloidal Films. Soft Matter. 2013; 9:3735–3740.

(11). Man W, Russel WB. Direct Measurements of Critical Stresses and Cracking in Thin Films of Colloid Dispersions. Phys Rev Lett. 2008; 100:198302. [PubMed: 18518494]

(12). Scherer GW. Theory of Drying. J Am Ceram Soc. 1990; 73:3–14.

(13). Nakahara A, Matsuo Y. Imprinting Memory into Paste to Control Crack Formation in Drying Process. J Stat Mech: Theory Exp. 2006; 2006:P07016.

(14). Fratzl P, Gupta HS, Fischer FD, Kolednik O. Hindered Crack Propagation in Materials with Periodically Varying Young's Modulus–Lessons from Biological Materials. Adv Mater. 2007; 19:2657–2661.

(15). Dugyala VR, Lama H, Satapathy DK, Basavaraj MG. Role of Particle Shape Anisotropy on Crack Formation in Drying of Colloidal Suspension. Sci Rep. 2016; 6:30708. [PubMed: 27477261]

(16). Winnik MA. Latex Film Formation. Curr Opin Colloid Interface Sci. 1997; 2:192–199.

(17). Almanza-Workman AM, Taussig CP, Jeans AH, Cobene RL. Fabrication of Three-Dimensional Imprint Lithography Templates by Colloidal Dispersions. J Mater Chem. 2011; 21:14185–14192.

(18). Boulogne F, Giorgiutti-Dauphiné F, Pauchard L. How to Reduce the Crack Density in Drying Colloidal Material? Oil Gas Sci Technol. 2014; 69:397–404.

(19). Smith MI, Sharp JS. Effects of Substrate Constraint on Crack Pattern Formation in Thin Films of Colloidal Polystyrene Particles. Langmuir. 2011; 27:8009–8017. [PubMed: 21650173]

(20). Tang X. Crack-Free TiO_2 Thin Films with Selfassembling Nano-Particles Fabricated Through In-Situ Sol–Gel Processing in Reverse Micelles. Surf Coat Technol. 2013; 221:37–43.

(21). Kappert EJ, Pavlenko D, Malzbender J, Nijmeijer A, Benes NE, Tsai PA. Formation and Prevention of Fractures in Sol–Gel-Derived Thin Films. Soft Matter. 2015; 11:882–888. [PubMed: 25466584]

(22). Prosser JH, Brugarolas T, Lee S, Nolte AJ, Lee D. Avoiding Cracks in Nanoparticle Films. Nano Lett. 2012; 12:5287–5291. [PubMed: 22984890]

(23). Wang L, Zhao XS. Fabrication of Crack-Free Colloidal Crystals Using a Modified Vertical Deposition Method. J Phys Chem C. 2007; 111:8538–8542.

(24). Santanach Carreras E, Chabert F, Dunstan EE, Franks GV. Avoiding “mud” Cracks During Drying of Thin Films from Aqueous Colloidal Suspensions. J Colloid Interface Sci. 2007; 313:160–168. [PubMed: 17521665]

(25). Kanai T, Sawada T. New Route to Produce Dry Colloidal Crystals Without Cracks. Langmuir. 2009; 25:13315–13317. [PubMed: 19874037]

(26). Kim JY, Cho K, Ryu S, Kim SY, Weon BM. Crack Formation and Prevention in Colloidal Drops. Sci Rep. 2015; 5:13166. [PubMed: 26279317]

(27). Schneider M, Koos E, Willenbacher N. Highly Conductive, Printable Pastes from Capillary Suspensions. Sci Rep. 2016; 6:31367. [PubMed: 27506726]

(28). Jin Q, Tan P, Schofield AB, Xu L. Eliminating Cracking During Drying. Eur Phys J E: Soft Matter Biol Phys. 2013; 36:28.

(29). Chiu RC, Cima MJ. Drying of Granular Ceramic Films: II, Drying Stress and Saturation Uniformity. J Am Ceram Soc. 1993; 76:2769–2777.

(30). Singh KB, Tirumkudulu MS. Cracking in Drying Colloidal Films. Phys Rev Lett. 2007; 98:218302. [PubMed: 17677816]

(31). Singh KB, Bhosale LR, Tirumkudulu MS. Cracking in Drying Colloidal Films of Flocculated Dispersions. Langmuir. 2009; 25:4284–4287. [PubMed: 19323451]

(32). Koos E, Willenbacher N. Capillary Forces in Suspension Rheology. Science. 2011; 331:897–900. [PubMed: 21330542]

(33). Koos E. Capillary Suspensions: Particle Networks Formed Through the Capillary Force. Curr Opin Colloid Interface Sci. 2014; 19:575–584. [PubMed: 25729316]

(34). Koos E, Willenbacher N. Particle Configuration and Gelation in Capillary Suspensions. Soft Matter. 2012; 8:3988–3994.

(35). Hoffmann S, Koos E, Willenbacher N. Using Capillary Bridges to Tune Stability and Flow Behavior of Food Suspensions. Food Hydrocolloids. 2014; 40:44–52.

(36). Wollgarten S, Yüce C, Koos E, Willenbacher N. Tailoring Flow Behavior and Texture of Water Based Cocoa Suspensions. Food Hydrocolloids. 2016; 52:167–174.

(37). Bitsch B, Dittmann J, Schmitt M, Scharfer P, Schabel W, Willenbacher N. A Novel Slurry Concept for the Fabrication of Lithium-Ion Battery Electrodes with Beneficial Properties. J Power Sources. 2014; 265:81–90.

(38). Zhang Y, Allen MC, Zhao R, Deheyn DD, Behrens SH, Meredith JC. Capillary Foams: Stabilization and Functionalization of Porous Liquids and Solids. Langmuir. 2015; 31:2669–2676. [PubMed: 25689577]

(39). Dittmann J, Koos E, Willenbacher N. Ceramic Capillary Suspensions: Novel Processing Route for Macroporous Ceramic Materials. J Am Ceram Soc. 2013; 96:391–397.

(40). Herminghaus S. Dynamics of Wet Granular Matter. Adv Phys. 2005; 54:221–261.

(41). Butt HJ, Kappl M. Normal Capillary Forces. Adv Colloid Interface Sci. 2009; 146:48–60. [PubMed: 19022419]

(42). Mehrotra VP, Sastry VS. Pendular Bond Strength Between Unequal-Sized Spherical Particles. Powder Technol. 1980; 25:203–214.

(43). Gao C. Theory of Menisci and Its Applications. Appl Phys Lett. 1997; 71:1801–1803.

(44). Butt HJ. Capillary Forces: Influence of Roughness and Heterogeneity. Langmuir. 2008; 24:4715–4721. [PubMed: 18442225]

(45). Megias-Alguacil D, Gauckler LJ. Capillary Forces Between Two Solid Spheres Linked by a Concave Liquid Bridge: Regions of Existence and Forces Mapping. AIChE J. 2009; 55:1103–1109.

(46). Brochard-Wyart F, Di Meglio JM, Quere D, de Gennes PG. Spreading of Non-volatile Liquids in a Continuum Picture. Langmuir. 1991; 7:335–338.

(47). Butt, HJ., Graf, K., Kappl, M. Physics and Chemistry of Interfaces. 3rd ed. Wiley-VCH; Weinheim, Germany: 2013.

(48). Yamamoto K, Tanuma C, Gemma N. Competition Between Electrostatic and Capillary Forces Acting on a Single Particle. Jpn J Appl Phys. 1995; 34:4176.

(49). Koos E, Kannowade W, Willenbacher N. Restructuring and Aging in a Capillary Suspension. Rheol Acta. 2014; 53:947–957. [PubMed: 25729113]

(50). Schubert H. Capillary Forces – Modeling and Application in Particulate Technology. Powder Technol. 1984; 37:105–116.

(51). Pietsch WB, Rumpf H. Haftkraft, Kapillardruck, Flüssigkeitsvolumen Und Grenzwinkel Einer Flüssigkeitsbrücke Zwischen Zwei Kugeln. Chem Ing Tech. 1967; 39:885–893.

(52). Weingärtner, H. Chemische Thermodynamik: Einführung Für Chemiker Und Chemieingenieure. Vieweg Verlag; Wiesbaden, Germany: 2003. p. 221

(53). Ho CK, Udell KS. Mass Transfer Limited Drying of Porous Media Containing an Immobile Binary Liquid Mixture. Int J Heat Mass Transfer. 1995; 38:339–350.

(54). Schwarzbach J, Schlünder EU. Fluidized Bed Drying of Materials Wetted with a Binary Liquid Mixture. Chem Eng Process. 1993; 32:13–32.

(55). Vogel H-J, Hoffmann H, Roth K. Studies of Crack Dynamics in Clay Soil: I. experimental Methods, Results, and Morphological Quantification. Geoderma. 2005; 125:203–211.

(56). Dittmann J, Willenbacher N. Micro Structural Investigations and Mechanical Properties of Macro Porous Ceramic Materials from Capillary Suspensions. J Am Ceram Soc. 2014; 97:3787–3792.

(57). Domenech T, Velankar SS. On the Rheology of Pendular Gels and Morphological Developments in Paste-like Ternary Systems Based on Capillary Attraction. Soft Matter. 2015; 11:1500–1516. [PubMed: 25582822]

(58). Chiu RC, Garino TJ, Cima MJ. Drying of Granular Ceramic Films: I, Effect of Processing Variables on Cracking Behavior. J Am Ceram Soc. 1993; 76:2257–2264.

(59). Bossler F, Koos E. Structure of Particle Networks in Capillary Suspensions with Wetting and Nonwetting Fluids. Langmuir. 2016; 32:1489–1501. [PubMed: 26807651]

(60). Tirumkudulu MS, Russel WB. Cracking in Drying Latex Films. Langmuir. 2005; 21:4938–4948. [PubMed: 15896034]

(61). Koos E, Johannsmeier J, Schwebler L, Willenbacher N. Tuning Suspension Rheology Using Capillary Forces. Soft Matter. 2012; 8:6620–6628.

(62). Xu L, Davies S, Schofield AB, Weitz DA. Dynamics of Drying in 3D Porous Media. Phys Rev Lett. 2008; 101:094502. [PubMed: 18851617]

(63). Günzler, H., Gremlich, HU. IR Spectroscopy: An Introduction. Wiley-VCH; 2002.

(64). Kumar PM, Badrinarayanan S, Sastry M. Nanocrystalline TiO_2 Studied by Optical, FTIR and X-Ray Photoelectron Spectroscopy: Correlation to Presence of Surface States. Thin Solid Films. 2000; 358:122–130.

(65). Gao Y, Masuda Y, Peng Z, Yonezawa T, Koumoto K. Room Temperature Deposition of a TiO_2 Thin Film from Aqueous Peroxotitanate Solution. J Mater Chem. 2003; 13:608–613.

(66). Demond AH, Lindner AS. Estimation of Interfacial Tension Between Organic Liquids and Water. Environ Sci Technol. 1993; 27:2318–2331.

(67). Lang BE. Solubility of Water in Octan-1-Ol from (275 to 369) K. J Chem Eng Data. 2012; 57:2221–2226.

(68). Vanderhoff JW, Bradford EB, Carrington WK. The Transport of Water Through Latex Films. J Polym Sci. 1973; 41:155–174.

(69). Routh AF. Drying of Thin Colloidal Films. Rep Prog Phys. 2013; 76:046603. [PubMed: 23502077]

(70). Su JT, Duncan PB, Momaya A, Jutila A, Needham D. The Effect of Hydrogen Bonding on the Diffusion of Water in *n*-Alkanes and *n*-Alcohols Measured with a Novel Single Microdroplet Method. J Chem Phys. 2010; 132:044506. [PubMed: 20113048]

(71). Florence, AT., Attwood, D. Physicochemical Principles of Pharmacy. 5th ed. Royal Pharmaceutical Society; London: 2011.

(72). Croll SG. Drying of Latex Paint. J Coat Technol. 1986; 58:41–49.

(73). Croll SG. Heat and Mass Transfer in Latex Paints During Drying. J Coat Technol. 1987; 59:81–92.

(74). Deegan RD, Bakajin O, Dupont TF, Huber G, Nagel SR, Witten TA. Capillary Flow As the Cause of Ring Stains from Dried Liquid Drops. Nature. 1997; 389:827–829.

(75). Yunker PJ, Still T, Lohr MA, Yodh AG. Suppression of the Coffee-Ring Effect by Shape-Dependent Capillary Interactions. Nature. 2011; 476:308–311. [PubMed: 21850105]

(76). Bossler F, Weyrauch L, Schmidt R, Koos E. Influence of Mixing Conditions on the Rheological Properties and Structure of Capillary Suspensions. Colloids Surf, A. 2017; 518:85–97.

(77). Caro J. Hierarchy in Inorganic Membranes. Chem Soc Rev. 2016; 45:3468–3478. [PubMed: 26466665]

(78). Last BJ, Thouless DJ. Percolation Theory and Electrical Conductivity. Phys Rev Lett. 1971; 27:1719–1721.

(79). Hauf K, Koos E. Herstellung Hochporöser Materialien Auf Basis Von Kapillarsuspensionen Mit Polymerbrücken. Chem Ing Tech. 2016; 88:1361.

(80). Dittmann J, Maurath J, Bitsch B, Willenbacher N. Highly Porous Materials with Unique Mechanical Properties from Smart Capillary Suspensions. Adv Mater. 2016; 28:1689–1696. [PubMed: 26677099]

Europe PMC Funders Author Manuscripts

Europe PMC Funders Author Manuscripts

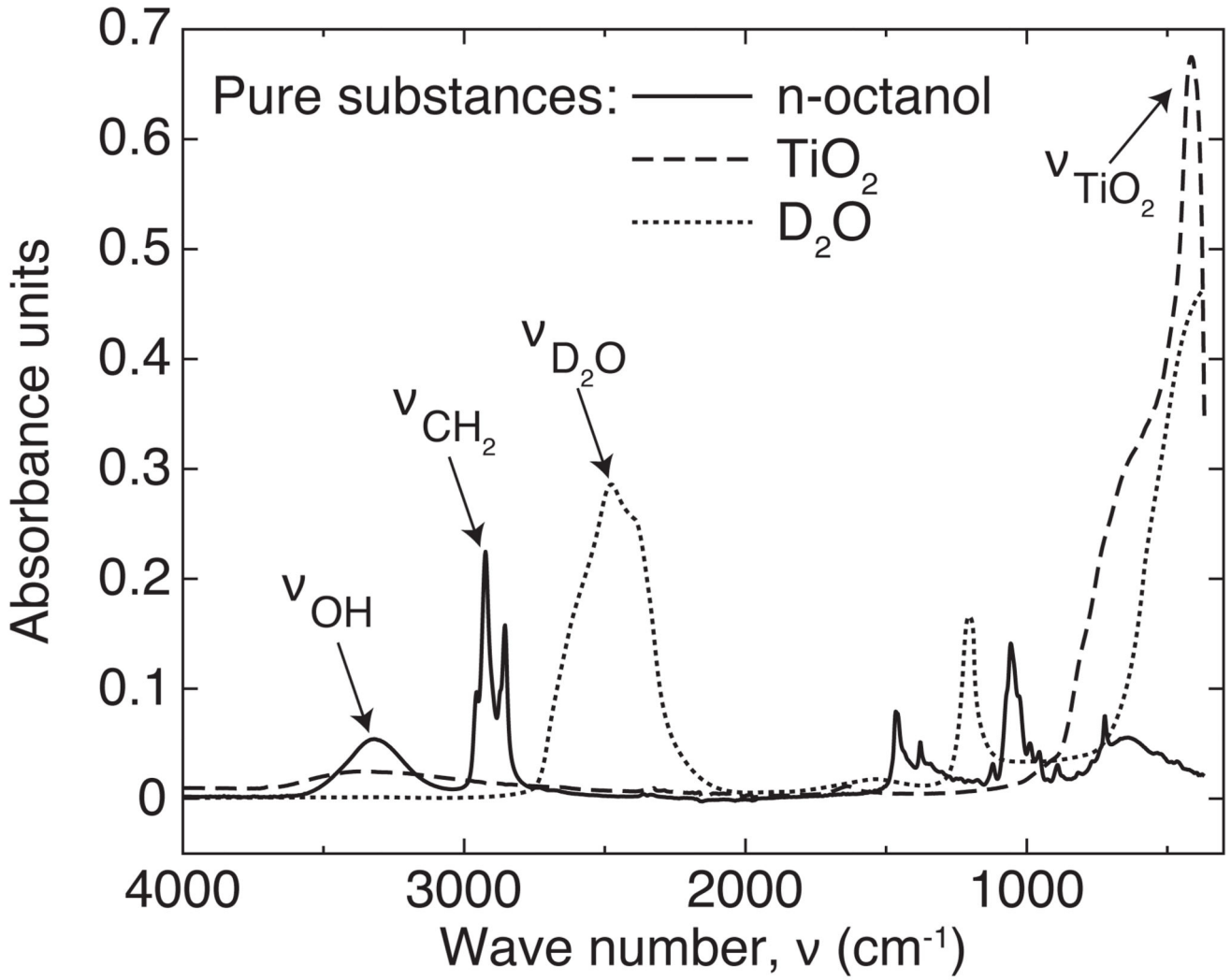

Figure 1.
Infrared absorbance spectra of the pure substances of the capillary suspension annotated with characteristic peaks for tracing the different substances

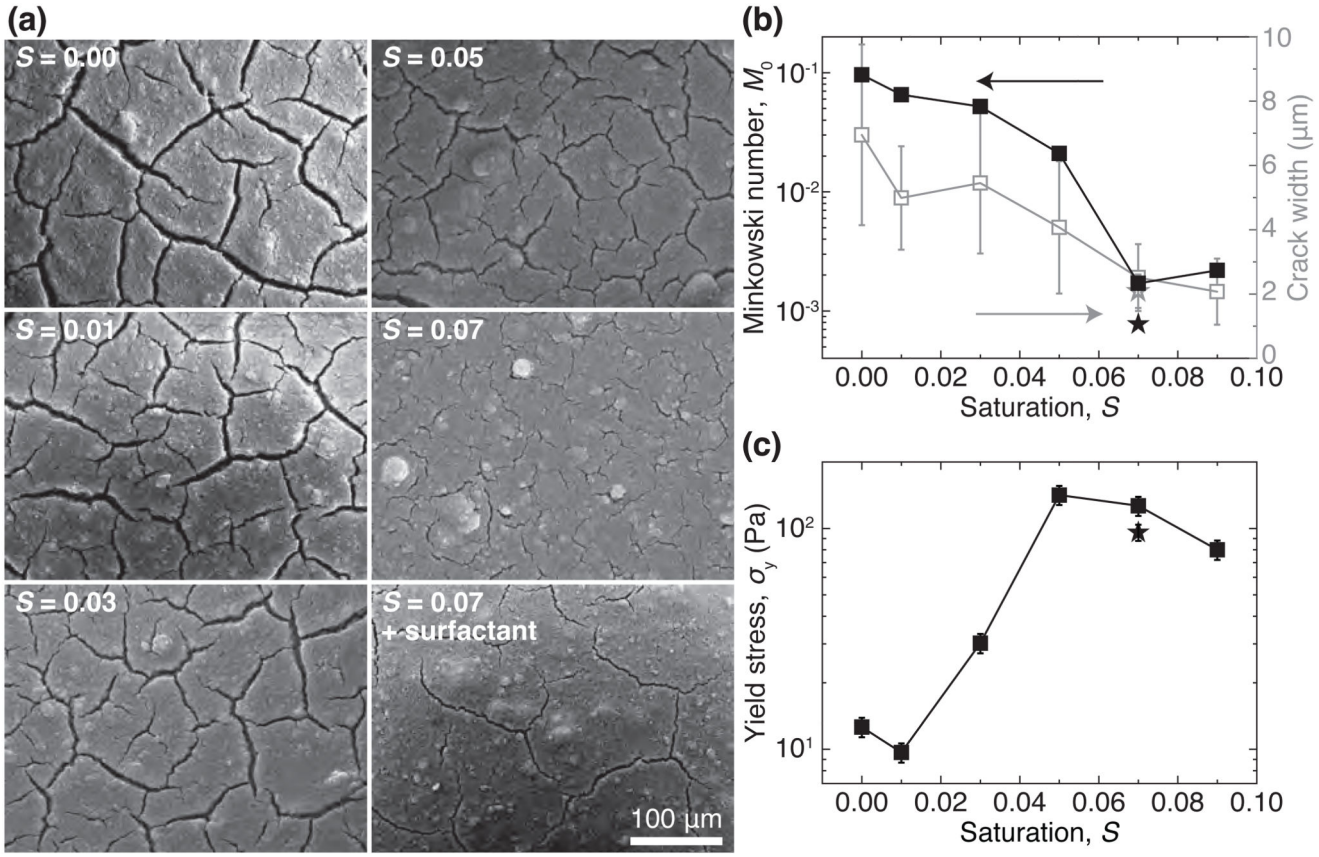

Figure 2.

(a) Surface morphology and (b) area density M_0 and average crack width after drying for TiO_2 particles dispersed in n-octanol with $\phi = 0.04$ and increasing amounts of secondary liquid S. (c) Yield stress σ_y versus saturation S for the TiO_2 suspensions prior to drying. The data point at $S = 0.07$ with 10 vol% Tego Dispers 752W in the secondary liquid is additionally shown in the lower right image and as a star in panels b and c.

Europe PMC Funders Author Manuscripts

Europe PMC Funders Author Manuscripts

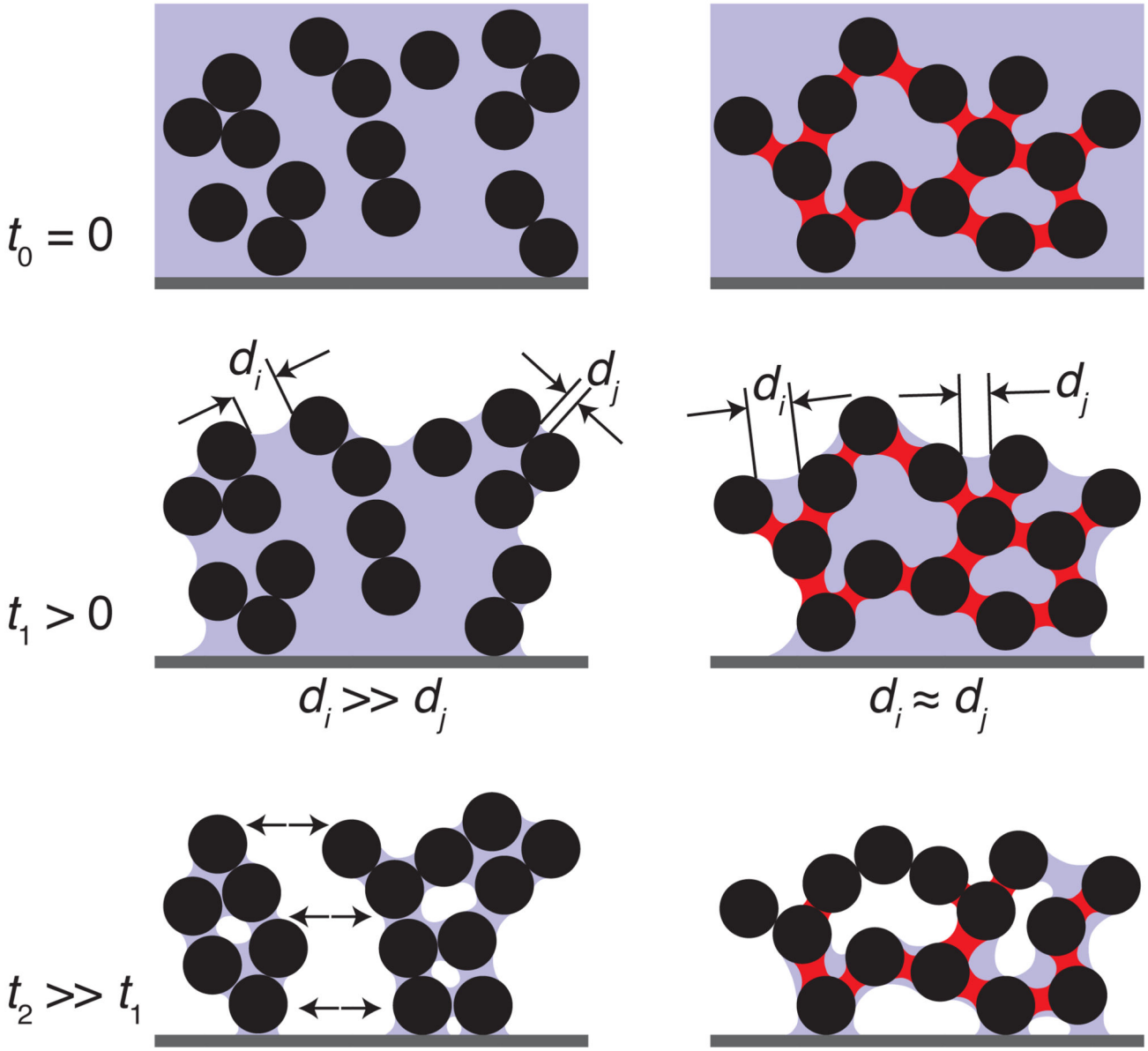

Figure 3.

Particle distribution in a nonstabilized particle suspension (*left*) and in a capillary suspension (*right*) at various times during drying where t_0 represents the initial time of coating, t_1 some later time as the film begins to dry, and t_2 the time when the film is nearly dry.

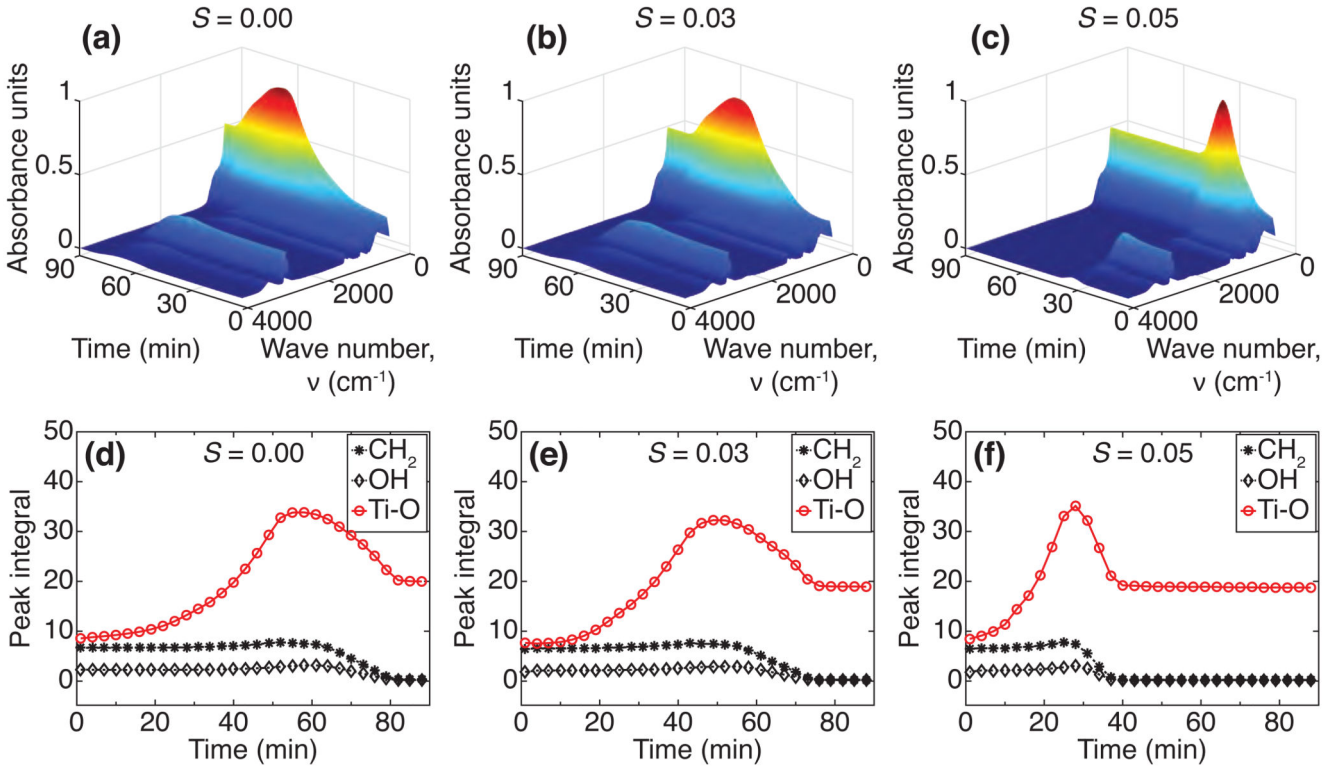

Figure 4.

(a-c) Infrared absorption spectra and (d-f) corresponding surface integrals (i.e., intensity) of characteristic n-octanol (CH_2 and OH) and Ti-O peaks for TiO_2 capillary suspensions with three different D_2O saturations as a function of drying time.

Europe PMC Funders Author Manuscripts

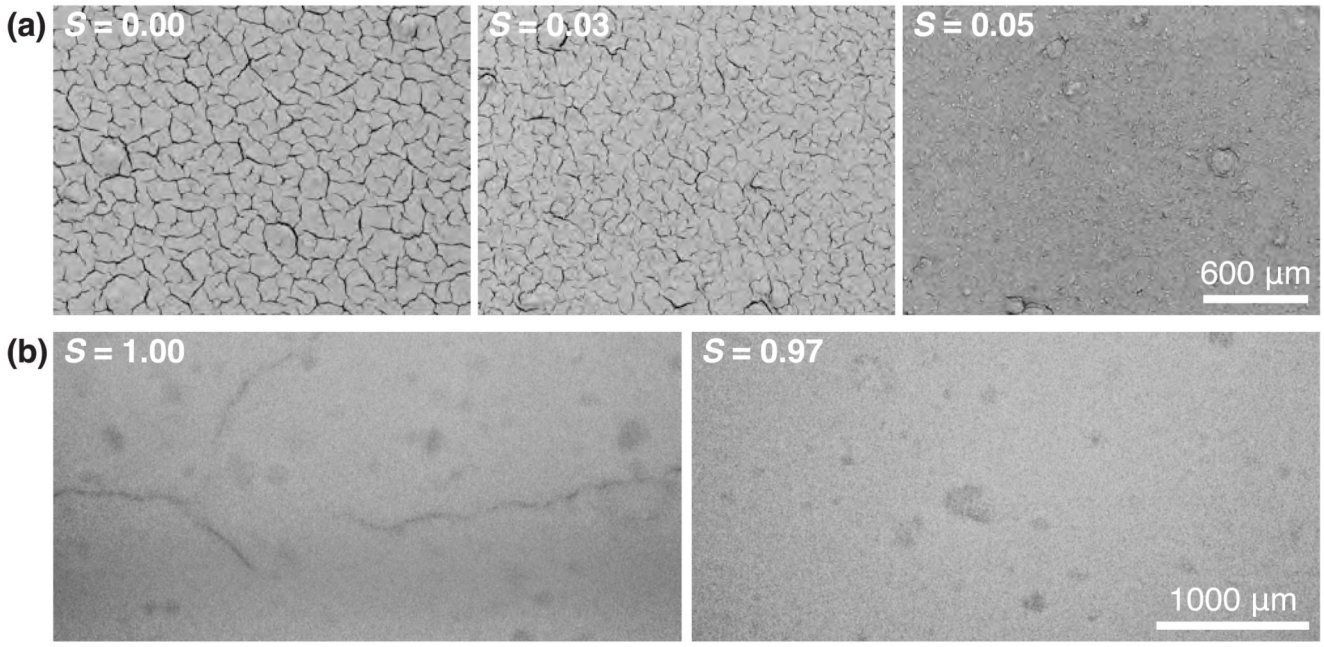

Figure 5.

Dry surface pattern of (a) the pendular state system using ZnO and (b) the capillary state system using $CaCO_3$ particles. ZnO was dispersed in n-octanol ($\phi = 0.05$) and stabilized as capillary suspension with H_2O at various saturations as specified in the images. Hydrophobically modified $CaCO_3$ was dispersed in n-octanol ($\phi = 0.10$) shown with and without added water.

Europe PMC Funders Author Manuscripts

Europe PMC Funders Author Manuscripts

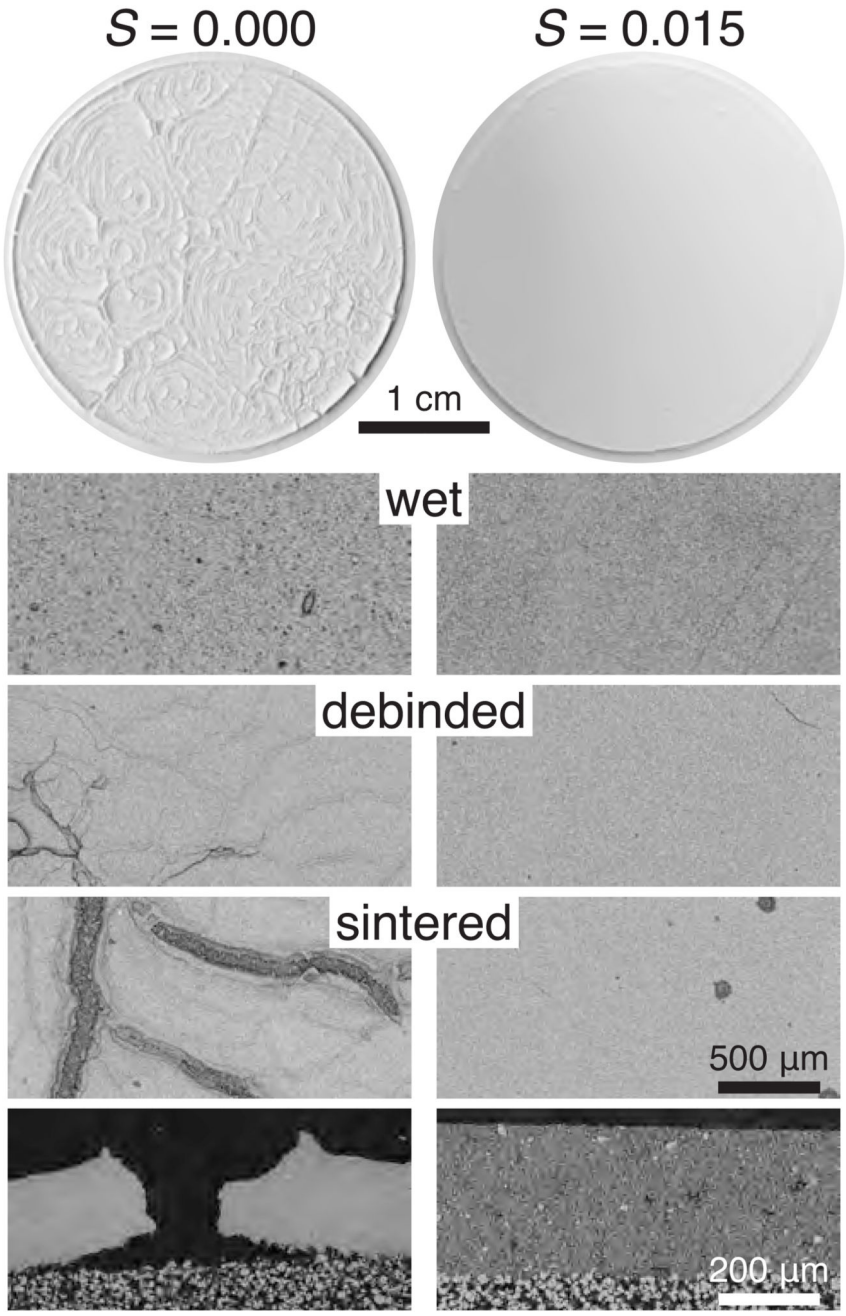

Figure 6.

Wet, debinded, and sintered Al_2O_3 ceramic layers with solid volume fraction $\phi = 0.15$ and with saturation (*left*) $S = 0.000$ and (*right*) $S = 0.015$. The bottom SEM images show a cut and polished portion of the sintered films. The diameter of the discs (shown after sintering) is 30 mm with a wet film thickness of 300 µm. The ceramic layers with $S = 0.000$ show strong crack formation after the debinding step and even partial delamination after sintering.

Europe PMC Funders Author Manuscripts

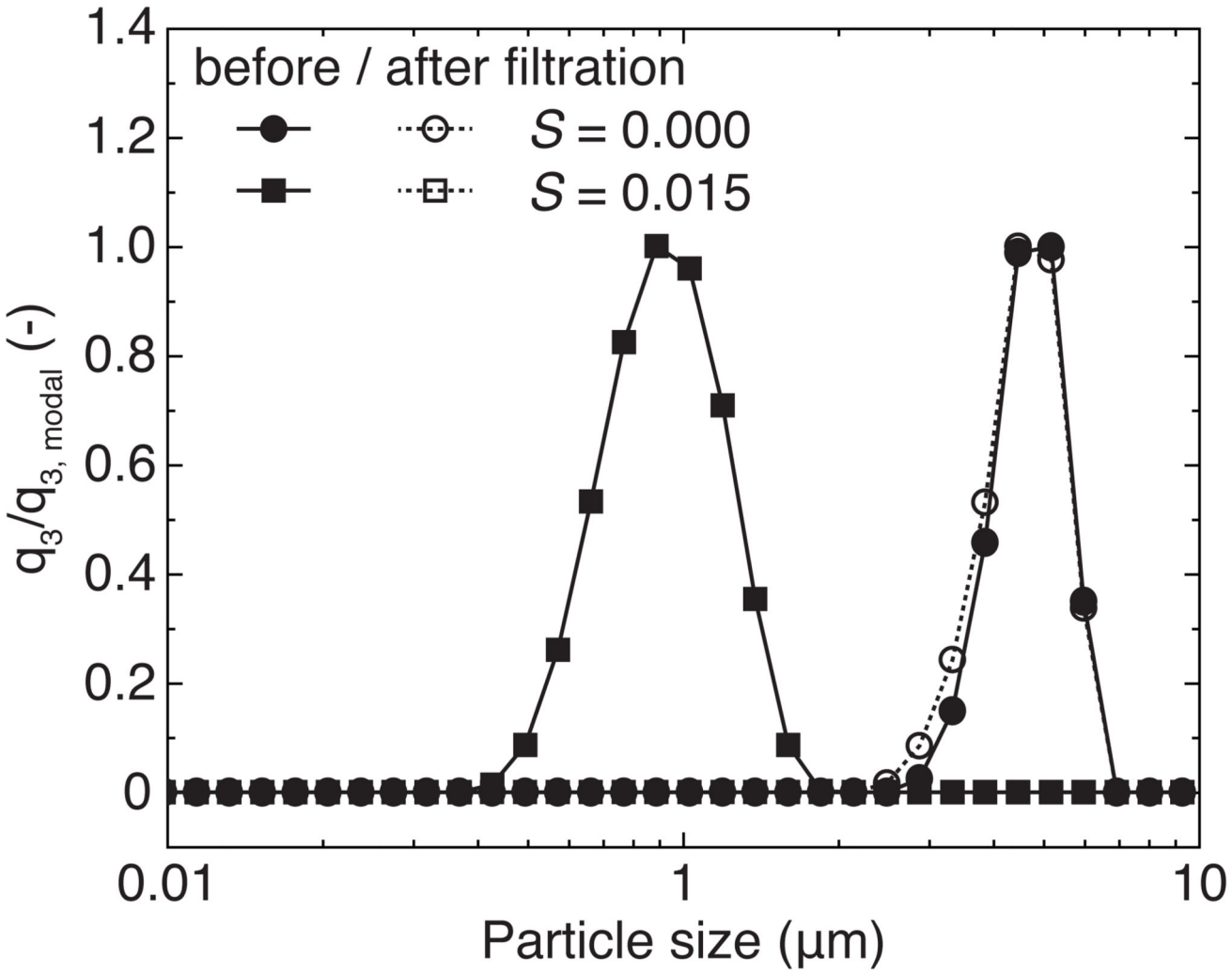

Figure 7.

Results of filtration tests for a crack-free capillary suspension membrane ($S = 0.015$) and a pure suspension membrane ($S = 0.000$) with large cracks. Both membranes had a wet thickness of 100 μm. Test suspensions were polystyrene particles in water. The particle size distributions shown here are normalized by the corresponding modal value of the size distribution. The crack free capillary suspension membrane successfully separates 1 μm polystyrene particles. The pure suspension membrane cannot even separate 5 μm particles.

Europe PMC Funders Author Manuscripts

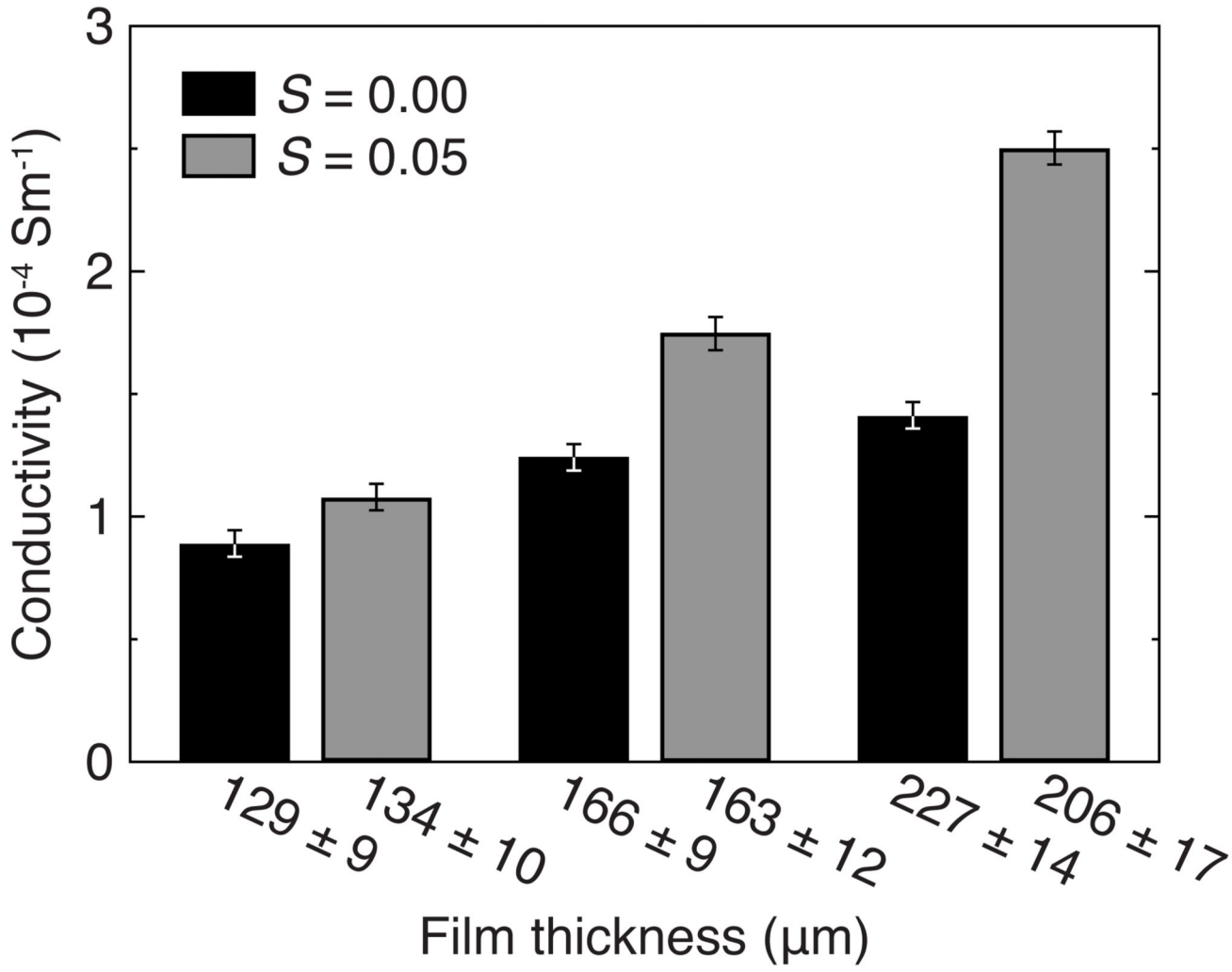

Figure 8.

Conductivity for unsintered nickel films at three thicknesses both without and with added liquid. The conductivity increases appreciably for the films produced from capillary suspensions as a function of the film height due to the increase in the area of the conductive pathway. This measured conductivity is lower for the films made from pure suspensions due to the partial cracking occurring in this case when the thickness exceeds 180 μm.